MRS Communications (2020), *10*, 636–641

doi:10.1557/mrc.2020.73

MRS Communications

Research Letter

Insensitivity of the extent of surface reduction of ceria on termination: comparison of (001), (110), and (111) faces

Weizi Yuan and **Sossina M. Haile**, Department of Materials Science and Engineering, Northwestern University, Evanston, IL 60208, USA
Address all correspondence to Sossina M. Haile at **sossina.haile@northwestern.edu**

(Received 17 July 2020; accepted 15 September 2020)

Abstract

The enhanced reducibility of the surface of ceria relative to the bulk has long been established. Several studies also show that ceria nanoparticles with different facets exhibit different catalytic activities. Despite consensus that the activity is correlated with the surface Ce^{3+} concentration, experimental measurements of this concentration as a function of termination are lacking. Here, X-ray absorption near-edge spectroscopy (XANES) is used to quantify the Ce^{3+} concentration in films with (001), (110), and (111) surface terminations under reaction relevant conditions. While an enhanced Ce^{3+} concentration is found at the surfaces, it is surprisingly insensitive to film orientation.

Introduction

Ceria is widely used as a catalyst for a range of industrially important chemical,[1] and increasingly, biomedical,[2] transformations. It is well-established that the surface of ceria, at which heterogeneous reactions are catalyzed, is substantially more reduced that the bulk.[3–5] This surface reducibility has been identified as a key factor in the catalytic activity.[6,7] In parallel, strong evidence has emerged that the activity of different facets of ceria can differ substantially, and in recent years, there has been an explosion in efforts to exploit this behavior.[7–10]

Studies of termination effects on ceria catalysis rates have largely focused on the three most stable faces, which occur with stability sequence (111) > (110) > (001).[11,12] Computational studies of these surfaces suggest oxygen vacancy formation energies increase in the order (110) > (001) > (111),[12] implying a decrease in vacancy concentrations in this sequence, which notably does not correlate with the stability sequence. Experimental investigations have leveraged shape-selective synthetic approaches that yield faceted ceria nanostructures dominated by one or the other of these terminations.[8–10] In particular, conditions can be tuned to yield ceria cubes which display {001} faces; octahedra, which display {111} faces; truncated octahedra which display {111} and {001} faces; and rods, which grow along the [110] direction and are terminated either primarily by {110} faces or by a combination of {001} and {110} faces.[2,8,9,13–18] Using such materials, the rates of a broad range of reactions catalyzed have been characterized,[10] including for example, the reaction between hydrogen peroxide and tetramethylbenzidine in aqueous solution,[2] photocatalytic degradation of methylene blue,[19] and fairly commonly, gas-phase oxidation of carbon monoxide.[20–22] Similarly, surface defect concentrations have been studied by a variety of techniques,[23,24] with X-ray photoemission electron spectroscopy (XPS)[2,19] and Raman spectroscopy[2,19,25] having been particularly widely exploited.

Based on these extensive studies, it is generally agreed upon that the activity of the various surfaces of ceria is directly correlated to the reducibility of the surface in question. Thus, the activity sequence of nanorods > nanocubes > nanooctahedra observed for a vast number of reactions is taken to result from the relative concentrations of oxygen vacancies on the facets that form these structures. An intriguing counterexample has been presented by Yang et al.,[2] who demonstrate that the exposed facets of ceria can influence reactivity in a manner than exceeds differences in surface vacancy concentrations. Thus, the impact and significance of termination may not be entirely settled. A number of factors, in fact, complicate studies aimed at elucidating the role of surface defect state on the catalytic activity of nanostructured ceria. The first is the inherent convolution of size effects with termination effects. That is, even for a given nanostructure morphology, a decrease in size results in an initial increase in oxygen vacancy concentration. The second is the near-impossibility of synthesizing nanostructures with just one termination. Consequently, quantification relies on assessing the detailed particle morphologies, typically as determined by electron microscopy. The third is the inevitable occurrence of edge sites, which can become particularly important as the particle size is decreased.

As a contribution toward unraveling the role of termination on the properties of ceria, we present here a study of well-defined ceria thin films with (001), (110), and (111) termination. We employ angle-resolved X-ray absorption near-edge spectroscopy (XANES)[5] to quantify the Ce^{3+} concentration in the top few nanometers of the films, as well as throughout

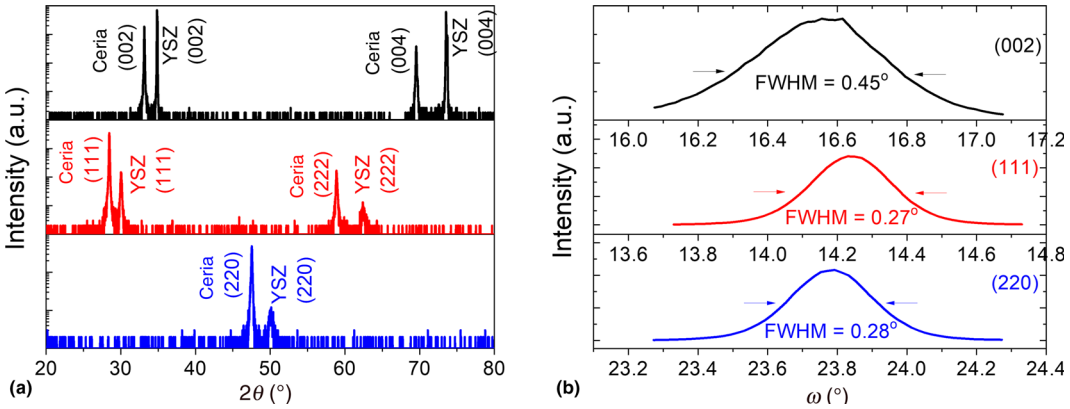

Figure 1. X-ray diffraction patterns of CeO_2 films (220 nm) on YSZ (001), (111), and (110): (a) specular θ–2θ scans and (b) rocking curves about the CeO_2 (002), (111), and (220). Data collected using a Cu K_α X-ray source (50 kV, 240 mA).

their bulk, under conditions relevant to high-temperature gas-phase catalysis. The technique is particularly well-suited to such a study because, unlike XPS and electron energy-loss spectroscopy (EELS), which can also be used to study oxidation state of material surfaces, a vacuum environment is not required and sample charging does not occur. In contrast to computational predictions, we find in this work a remarkable insensitivity of the Ce^{3+} concentration, and from that the inferred oxygen vacancy concentration, to film termination, but a detectable sensitivity to orientation of the number of accessible high-energy electron states.

Film growth

Epitaxial films of CeO_2, 220 nm in thickness, were grown on $Y_{0.16}Zr_{0.84}O_{1.92}$ (yttria-stabilized zirconia, YSZ) substrates of three different orientations: (001), (110), and (111).[26,27] In the specular θ–2θ diffraction patterns, Fig. 1(a), only the peaks consistent with the desired orientation are evident. The rocking curves, Fig. 1(b), display full width at half maximum (FWHM) values that range between 0.27° and 0.45°, as compared to the 0.02° of the substrate, reflective of the ~5.3% lattice mismatch between the substrate and the film. We have shown elsewhere,[5] by measuring the properties of similar films grown on *r*-sapphire, that there is no measurable impact of strain or in-plane domain size on the extent of surface reduction.

Surface and bulk oxidation state

XANES measurements were carried out at the Ce L_3 edge. Surface sensitivity was achieved by setting the incident angle, α, to 0.23°, a value that is smaller than the critical angle, $\theta_c \sim 0.45°$. When $\alpha < \theta_c$, X-ray total reflection occurs, and the X-ray penetration depth for the energies used is 2–3 nm. Moreover, the change in penetration depth on passing through the absorption edge is no more than about 1 nm. Bulk sensitivity was achieved by setting $\alpha = 10°$, at which the penetration depth exceeds the 220 nm thickness of the films. The moderate film thickness limits self-absorption effects which otherwise complicate quantitative analysis. Data were collected under three environmental conditions: ambient air at room temperature, ambient air at 800 °C, and low oxygen partial pressure ($pO_2 = 3.5 \times 10^{-13}$ mTorr) at 800 °C. The Ce^{3+} concentration was quantified using the linear combination fitting (LCF) method, as described in detail in a previous study.[5] The bulk ($\alpha = 10°$) film spectra collected at the temperature of interest and under air served as the reference for the fully oxidized state. Analogous measurements for $CeAlO_3$, as reported elsewhere,[5] were performed to obtain reference spectra for Ce fully in the 3+ oxidation state.

Representative XANES spectra from the bulk and surface regions of the (111) oriented film are presented in Fig. 2(a). A dramatic difference in bulk and surface spectra is immediately evident, with a downward shift in energies of the two main peaks (identified as A and B) of the surface spectrum, indicating a conspicuously reduced surface. Such behavior was noted also in our previous study of (001) oriented ceria–zirconia films.[5] The linear combination fits, Figs. 2(b) and 2(c), represent the experimental data well, capturing the reduction behavior. Moreover, the bulk Ce^{3+} concentration derived from the analysis, 1.1 ± 0.4 to $1.2 \pm 1.1\%$ (across all three films for this condition), is in agreement with the value of 1.1% derived from thermogravimetric measurements.[28] The complete set of results, Fig. 3, reveal that the surface spectra differ visibly between different orientations, whereas the bulk spectra are essentially identical to one another. However, the differences between the surface spectral features of different terminations are limited to the normalized absorbance intensities, with no significant differences in absorption energies. This result indicates that, rather remarkably, the Ce oxidation state (reflected in the edge energy) is unchanged for different facets. Instead, the number of accessible, higher-energy empty states, and hence, the ease or frequency of electron

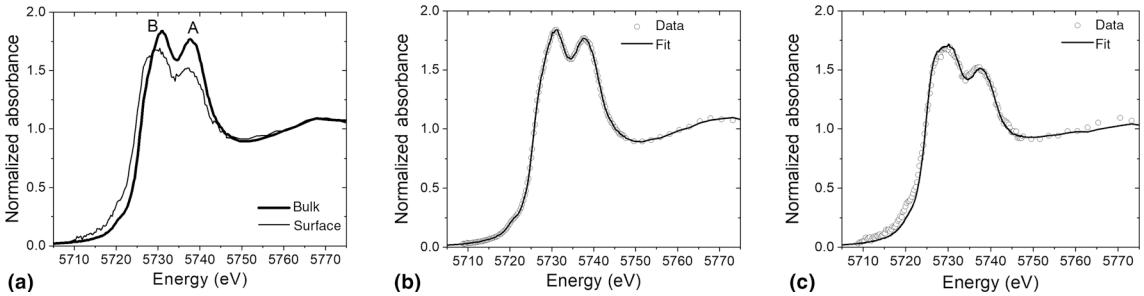

Figure 2. Representative and summary XANES results from ceria (111) thin films measured at 800 °C under pO_2 ~3.5×10^{-13} mTorr: (a) comparison of surface- and bulk-sensitive spectra; and comparison of measured and LCF fit spectra for (b) surface-sensitive and (c) bulk-sensitive measurements.

excitation into those states by the incident photon flux (reflected in the normalized intensity), is facet-dependent.[29]

The Ce^{3+} concentration derived from the LCF analysis and the heights of the A and B peaks of the surface spectra are summarized in Fig. 4. The error bars in the Ce^{3+} concentrations in Fig. 4(a) are derived from the difference between the fit and measured spectra.[5] A return to the initial conditions at the completion of the high-temperature experiments fully reproduced the initial bulk spectra as well as the results of the LCF analysis for both bulk and surface regions, eliminating film evolution over the course of the experiment as a possible explanation for the measured behavior.

Considering in some detail first the results of the LCF analysis, Fig. 4(a), under air, at both ambient temperature and 800 °C, 16 ± 5% of the Ce in the near-surface region is reduced to Ce^{3+}, and the difference between different terminations is less than 1% (of the total Ce content). A decrease in oxygen partial pressure to 3.5×10^{-13} mTorr at 800 °C induces an increase in the surface Ce^{3+} concentration to ~25%, and the differences between the different orientations are smaller than the ~5% uncertainty from the LCF fitting. In contrast to the insensitivity to film orientation, a change in oxygen partial pressure produces large changes in Ce^{3+} concentration. Shown for reference in Fig. 4(a) is the result for an (001) terminated film under an oxygen partial pressure of 7.4×10^{-14} mTorr (at 800 °C). While the impact on the bulk Ce^{3+} concentration is negligible, this condition increases the Ce^{3+} surface concentration to a remarkable 60%. The phase boundary of the defect fluorite region of the Ce_2O_3–CeO_2 phase diagram extends to about 50% Ce^{3+} at 800 °C,[30] rendering a change in phase unlikely to account for the similarities in the reduction extents of the different terminations.

Turning to the peak intensity summary, here an impact of termination is evident. The behavior is described as I(110) > I(001) ≈ I(111) at ambient temperature and I(110) > I(001) > I(111) at 800 °C. The latter, which is likely to hold also at the more moderate temperatures at which typical catalytic transformations are performed,[7–10] coincides with the chemical activity sequence noted in the catalysis community. Furthermore, the (110) termination retains its high absolute intensity at high temperature and reducing conditions, whereas absorption peak intensities for the (001) and (111) terminations decline strongly, much more strongly than the influence of thermal broadening evident for the bulk spectra. On return to the initial condition (air, ambient temperature), the high intensities are recovered, although they do not exactly match the initial measurement.

Overall, these results reveal that termination (or film orientation) has negligible impact on the Ce^{3+} concentration at the surface, but that termination has a small, non-negligible effect on the number of accessible, empty higher energy states. These observations suggest a reexamination of the underlying mechanism by which termination effects influence the rate of heterogeneous reactions on ceria surfaces. In parallel, efforts to determine surface atomic structure and to measure defect concentrations with greater precision are certainly warranted. For example, it is possible that surface oxygen vacancy concentration may, in fact, be smaller than half the Ce^{3+} concentration if the electronic Ce^{3+} defects are charge compensated (at least in part) by surface hydroxyl groups, as has been observed for ceria surfaces characterized at somewhat lower temperatures than examined here.[31] Further studies will be required to unravel the relationship between the nature of extrinsic surface adsorbed species, intrinsic surface defect concentrations, surface electronic structure, and crystallographic facet.

Methods

Films were grown by pulsed laser deposition (PLD). A CeO_2 target for PLD film growth was synthesized from commercial powder (99.9% purity, Sigma-Aldrich #211575, St. Louis, MO, USA). The powder was compacted under uniaxial pressure and sintered at 1500 °C for 10 h under still air. $Y_{0.16}Zr_{0.84}O_{1.92}$ (YSZ) substrates of three different orientations: (001), (110), and (111) were procured from MTI Corp (Richmond, CA, USA). Films were grown using a PVD (Wilmington, MA, USA) PLD/MBE 2300 instrument (KrF 248 nm excimer laser, 1.75 J/cm^2, 10 Hz repetition rate). During growth, the temperature of the substrate was fixed at 700 °C and the atmosphere was fixed at 30 mTorr of oxygen. At the conclusion of the deposition, the oxygen pressure was

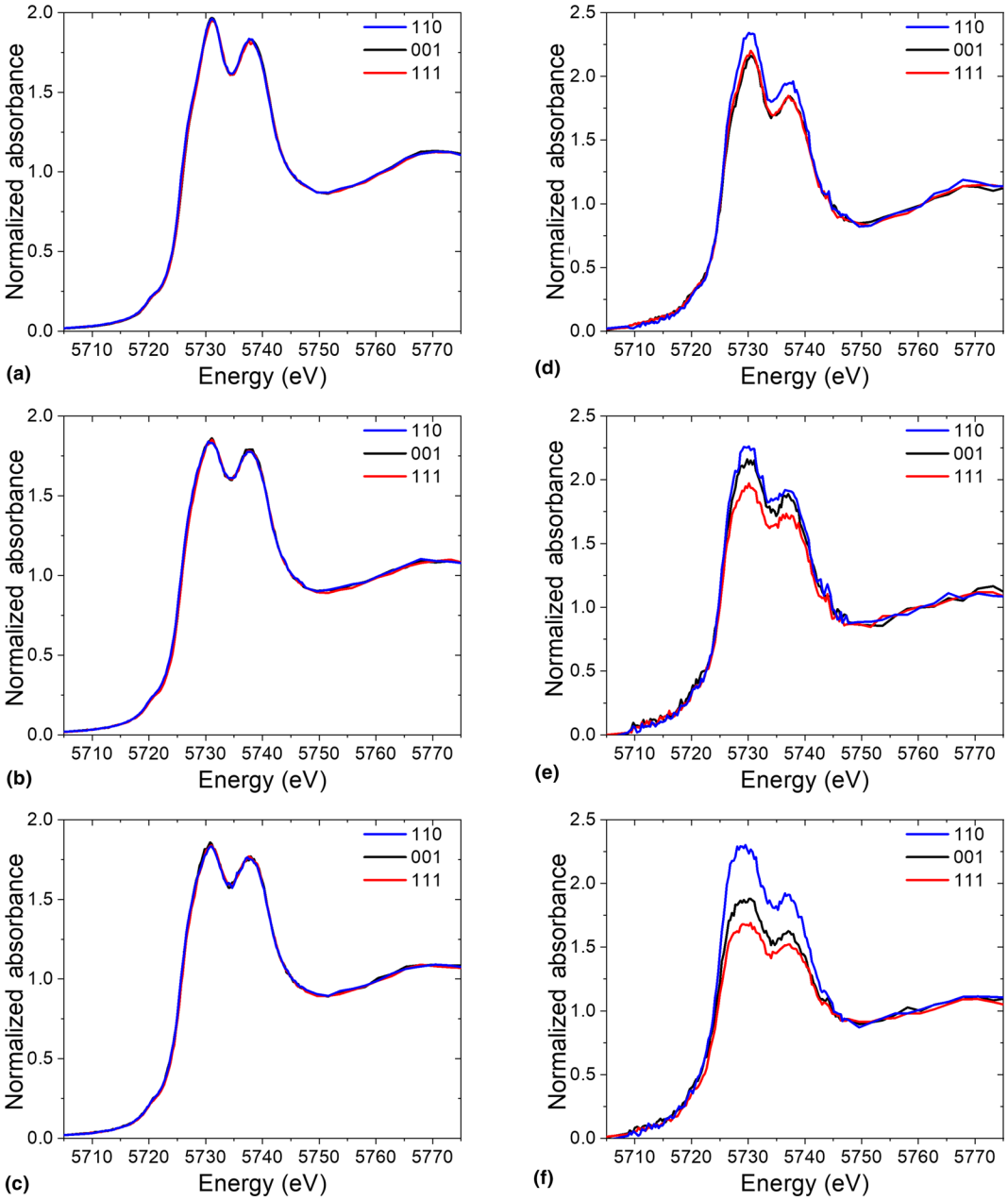

Figure 3. Normalized Ce L_3 edge XANES for ceria films: (a–c) bulk spectra and (d–f) surface spectra, with (a,d) at RT, under air; (b,e) at 800 °C, under air; and (c,f) at 800 °C under H_2/He (pO_2 ~3.5×10^{-13} mTorr).

raised to 250 Torr and the film then cooled at a rate of 10 °C/min to room temperature. Both specular θ–2θ X-ray diffraction scans and rocking curves were collected using a Rigaku (Tokyo, Japan) ATXG (Cu K_α).

XANES data were collected at DND-CAT 5BM-D station, at the Advanced Photon Source of Argonne National Laboratory, using a Si (111) double-crystal monochromator with an energy resolution of $\Delta E/E = 1.4 \times 10^{-4}$. The incident X-ray beam intensity was monitored by an ion chamber and was detuned to 60% of the maximum. The incident X-ray beam size was 0.05 (vertical) × 5 (horizontal) mm^2. Two Hitachi (Tokyo, Japan) Vortex-ME4 silicon drift detectors, set at 90° relative to the incident X-ray beam direction, were used to collect the fluorescence signal. Environmental conditions were controlled using an Anton Paar (Graz, Austria) (DHS1100) dome apparatus. The low oxygen partial pressure condition of 3.5×10^{-13} mTorr was obtained by bubbling 3.1% H_2 (balance He) through H_2O (held at 25 °C).

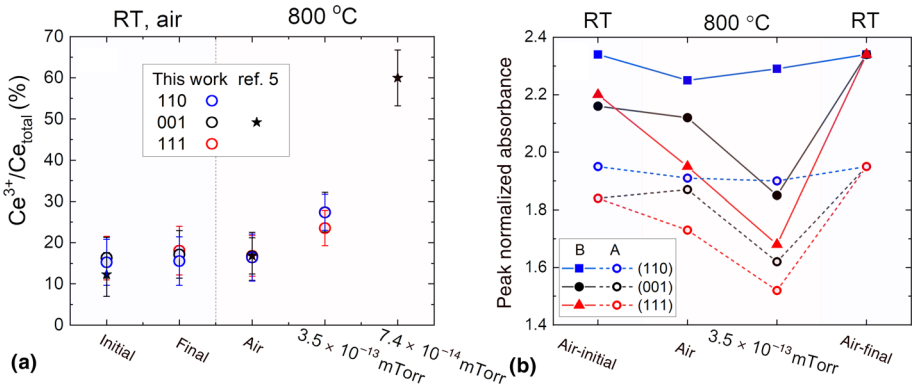

Figure 4. Summary of spectral characteristics of the surfaces of ceria films: (a) Ce^{3+} concentration as a function of environmental conditions and surface termination and (b) peak intensities of the absorbance peaks A and B (positions indicated in Fig. 2(a). In (a), data from previous measurements of (111) terminated ceria[5] are included. For ease of comparison, initial and final values are presented next to each other in (a), whereas the temporal sequence of experiments is emphasized in (b).

Acknowledgments

This work was supported primarily by NSF DMR-1505103. The XANES experiments were performed at the DuPont-Northwestern-Dow Collaborative Access Team (DND-CAT) located at Sector 5 of the Advanced Photon Source (APS). DND-CAT is supported by Northwestern University, E.I. DuPont de Nemours & Co., and The Dow Chemical Company. This research used resources of the Advanced Photon Source, a U.S. Department of Energy (DOE) Office of Science User Facility operated for the DOE Office of Science by Argonne National Laboratory under Contract No. DE-AC02-06CH11357. Part of this work made use of the Pulsed Laser Deposition Shared Facility and the X-ray Diffraction Facility at the Materials Research Center at Northwestern University, supported by the National Science Foundation MRSEC program (DMR-1720139) and the Soft and Hybrid Nanotechnology Experimental (SHyNE) Resource (NSF ECCS-1542205).

References

1. A. Trovarelli: Catalytic properties of ceria and CeO_2-containing materials. *Catal. Rev.* **38**, 439-520 (1996).
2. Y.S. Yang, Z. Mao, W.J. Huang, L.H. Liu, J.L. Li, J.L. Li, and Q.Z. Wu: Redox enzyme-mimicking activities of CeO_2 nanostructures: intrinsic influence of exposed facets. *Sci. Rep.* **6** no. 35344 (7 pp) (2016).
3. T.X.T. Sayle, S.C. Parker, and C.R.A. Catlow: The role of oxygen vacancies on ceria surfaces in the oxidation of carbon monoxide. *Surf. Sci.* **316**, 329-336 (1994).
4. Z. Zhao, M. Uddi, N. Tsvetkov, B. Yildiz, and A.F. Ghoniem: Redox kinetics study of fuel reduced ceria for chemical-looping water splitting. *J. Phys. Chem. C* **120**, 16271-16289 (2016).
5. W. Yuan, Q. Ma, Y. Liang, C. Sun, K.V.L.V. Narayanachari, M.J. Bedzyk, I. Takeuchi, and S.M. Haile: Unexpected trends in the enhanced Ce^{3+} surface concentration in ceria–zirconia catalyst materials. *J. Mater. Chem. A* **8**, 9850-9858 (2020).
6. D.R. Mullins: The surface chemistry of cerium oxide. *Surf. Sci. Rep.* **70**, 42-85 (2015).
7. A. Trovarelli and J. Llorca: Ceria catalysts at nanoscale: how do crystal shapes shape catalysis? *ACS Catal.* **7**, 4716-4735 (2017).
8. Z.A. Qiao, Z.L. Wu, and S. Dai: Shape-controlled ceria-based nanostructures for catalysis applications. *ChemSusChem* **6**, 1821-1833 (2013).
9. D.S. Zhang, X.J. Du, L.Y. Shi, and R.H. Gao: Shape-controlled synthesis and catalytic application of ceria nanomaterials. *Dalton Trans.* **41**, 14455-14475 (2012).
10. C.W. Sun, H. Li, and L.Q. Chen: Nanostructured ceria-based materials: synthesis, properties, and applications. *Energy Environ. Sci.* **5**, 8475-8505 (2012).
11. J. Paier, C. Penschke, and J. Sauer: Oxygen defects and surface chemistry of ceria: quantum chemical studies compared to experiment. *Chem. Rev.* **113**, 3949-3985 (2013).
12. M. Nolan, S.C. Parker, and G.W. Watson: The electronic structure of oxygen vacancy defects at the low index surfaces of ceria. *Surf. Sci.* **595**, 223-232 (2005).
13. Z. Liu, X.J. Li, M. Mayyas, P. Koshy, J.N. Hart, and C.C. Sorrell: Growth mechanism of ceria nanorods by precipitation at room temperature and morphology-dependent photocatalytic performance. *CrystEngComm* **19**, 4766-4776 (2017).
14. Z. Liu, X.J. Li, M. Mayyas, P. Koshy, J.N. Hart, and C.C. Sorrell: Growth mechanism of ceria nanorods by precipitation at room temperature and morphology-dependent photocatalytic performance (vol 19, pg 4766, 2017). *CrystEngComm.* **19**, 5492-5492 (2017).
15. E. Aneggi, D. Wiater, C. de Leitenburg, J. Llorca, and A. Trovarelli: Shape-dependent activity of ceria in soot combustion. *ACS Catal.* **4**, 172-181 (2014).
16. C.S. Pan, D.S. Zhang, L.Y. Shi, and J.H. Fang: Template-free synthesis, controlled conversion, and CO oxidation properties of CeO_2 nanorods, nanotubes, nanowires, and nanocubes. *Eur. J. Inorg. Chem.* **15**, 2429-2436 (2008).
17. Z.L. Wang and X.D. Feng: Polyhedral shapes of CeO_2 nanoparticles. *J. Phys. Chem. B* **107**, 13563-13566 (2003).
18. S.L. Chen, T. Cao, Y.X. Gao, D. Li, F. Xiong, and W.X. Huang: Probing surface structures of CeO_2, TiO_2, and Cu_2O nanocrystals with CO and CO_2 chemisorption. *J. Phys. Chem. C* **120**, 21472-21485 (2016).
19. Z. Liu, X.J. Li, M. Mayyas, P. Koshy, J.N. Hart, and C.C. Sorrell: Planar-dependent oxygen vacancy concentrations in photocatalytic CeO_2 nanoparticles. *CrystEngComm* **20**, 204-212 (2018).
20. X. Wang, Z.Y. Jiang, B.J. Zheng, Z.X. Xie, and L.S. Zheng: Synthesis and shape-dependent catalytic properties of CeO_2 nanocubes and truncated octahedra. *CrystEngComm* **14**, 7579-7582 (2012).
21. Z.L. Wu, M.J. Li, and S.H. Overbury: On the structure dependence of CO oxidation over CeO_2 nanocrystals with well-defined surface planes. *J. Catal.* **285**, 61-73 (2012).

22. S. Carrettin, P. Concepcion, A. Corma, J.M.L. Nieto, and V.F. Puntes: Nanocrystalline CeO_2 increases the activity of Au for CO oxidation by two orders of magnitude. *Angew. Chem. Int. Ed.* **43**, 2538-2540 (2004).
23. S. Turner, S. Lazar, B. Freitag, R. Egoavil, J. Verbeeck, S. Put, Y. Strauven, and G. Van Tendeloo: High resolution mapping of surface reduction in ceria nanoparticles. *Nanoscale* **3**, 3385-3390 (2011).
24. V.K. Paidi, L. Savereide, D.J. Childers, J.M. Notestein, C.A. Roberts, and J. van Lierop: Predicting NO_x catalysis by quantifying Ce^{3+} from surface and lattice oxygen. *ACS Appl. Mater. Interfaces* **9**, 30670-30678 (2017).
25. Z.L. Wu, M.J. Li, J. Howe, H.M. Meyer, and S.H. Overbury: Probing defect sites on CeO_2 nanocrystals with well-defined surface planes by Raman spectroscopy and O_2 adsorption. *Langmuir* **26**, 16595-16606 (2010).
26. W.C. Chueh, Y. Hao, W. Jung, and S.M. Haile: High electrochemical activity of the oxide phase in model ceria-Pt and ceria-Ni composite anodes. *Nat. Mater.* **11**, 155-161 (2012).
27. W.C. Chueh and S.M. Haile: Electrochemical studies of capacitance in cerium oxide thin films and its relationship to anionic and electronic defect densities. *Phys. Chem. Chem. Phys.* **11**, 8144-8148 (2009).
28. R.J. Panlener, R.N. Blumenthal, and J.E. Garnier: A thermodynamic study of nonstoichiometric cerium dioxide. *J. Phys. Chem. Solids* **36**, 1213-1222 (1975).
29. G.S. Henderson, F.M.F. de Groot, and B.J.A. Moulton: X-ray Absorption Near-Edge Structure (XANES) Spectroscopy *Reviews in Mineralogy and Geochemistry* **78**, 75–138 (2014).
30. H.J. Seifert, P. Nerikar, and H.L. Lukas: Thermodynamic assessment of the Ce-O system in solid state from 60 to 67 mol% O. *Int. J. Mater. Res.* **97**, 744-752 (2006).
31. Z.L.A. Feng, F. El Gabaly, X.F. Ye, Z.X. Shen, and W.C. Chueh: Fast vacancy-mediated oxygen ion incorporation across the ceria-gas electrochemical interface. *Nat. Commun.* **5** no. 4374 (9 pp) (2014).